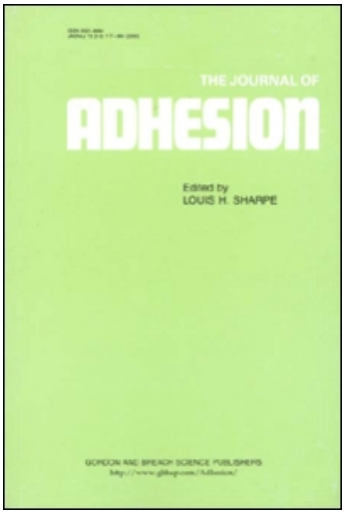

The Journal of Adhesion
Publication details, including instructions for authors and subscription information:
http://www.informaworld.com/smpp/title~content=t713453635

Relationship between Viscoelastic and Peeling Properties of Model Adhesives. Part 1. Cohesive Fracture

C. Derail[a]; A. Allal[a]; G. Marin[a]; Ph. Tordjeman[b]
[a] Laboratoire de Physique des Matériaux Industriels, Université de Pau et des Pays de l'Adour, Pau, France [b] ElfAtochem, Groupement de Recherches de Lacq, Lacq, France

To cite this Article Derail, C. , Allal, A. , Marin, G. and Tordjeman, Ph.(1997) 'Relationship between Viscoelastic and Peeling Properties of Model Adhesives. Part 1. Cohesive Fracture', The Journal of Adhesion, 61: 1, 123 — 157
To link to this Article: DOI: 10.1080/00218469708010519
URL: http://dx.doi.org/10.1080/00218469708010519

J. Adhesion, 1997, Vol. 61, pp. 123–157
Reprints available directly from the publisher
Photocopying permitted by license only

Relationship between Viscoelastic and Peeling Properties of Model Adhesives. Part 1. Cohesive Fracture

C. DERAIL[a], A. ALLAL[a], G. MARIN[a,*] and Ph. TORDJEMAN[b]

[a]*Laboratoire de Physique des Matériaux Industriels, Université de Pau et des Pays de l'Adour, 64000 Pau, France;*
[b]*ElfAtochem, Groupement de Recherches de Lacq, 64170 Lacq, France*

(Received 15 March 1996; In final form 14 May 1996)

The viscoelastic and peeling properties of polybutadiene/tackifying resin compatible blends have been studied in detail. Viscoelastic properties have been described through the variations of the complex shear modulus, $G^*(\omega)$, as a function of frequency, ω and peeling properties through the variations of peeling force (F) as a function of peeling rate (V).

After showing the objective character of the peeling curves obtained, the variations of the peeling force and peeling geometry have been studied as a function of volume fraction of the tackifying resin.

In this first paper, the analysis is focused on the first domain of the peeling curves, *i.e.* the cohesive fracture region. In this region, the peeling properties have been related to the viscoelastic properties in the terminal region of relaxation. It is shown that the longest relaxation time, τ_ρ, is a reducing parameter of the peeling curves, so a peeling master curve-which is independent of temperature, resin volume fraction and polymer molecular weight-may be defined. Furthermore, the variations of the test geometry as a function of peeling rate have been investigated: the variations of the radius of curvature of the aluminium foil have been analyzed with respect to the viscoelastic behavior of the adhesive, which in fact governs the test geometry.

A detailed analysis of all these features leads to a model which allows one to calculate the peeling curves in the cohesive domain from the adhesive formulation.

Keywords: Model hot-melt adhesives; adhesive joints; peeling; viscosity; rheology; master curves; rate dependence of failure mode; effect of geometry on failure; theory; experiment

INTRODUCTION

There has been a strong increase in the market for hot-melt adhesives in the last few years, with the development of new applications due to

*Corresponding author.

the continuous improvement and fitting of the properties of adhesive formulations. The design of the formulation of a hot-melt adhesive proceeds largely from "rules of thumb" that depend mostly on the intuition and experience of the formulators and also a good knowledge of the properties of the individual components of the blends.

The relationship between peeling and adhesive properties of pressure sensitive and hot-melt adhesives has been extensively studied in the last 20 years: the most striking result is maybe the fact that a peeling curve is a rheological curve obeying the time-temperature superposition principle. Whatever the fracture mode (cohesive or interfacial) one may, in most cases, define for the peeling data a temperature shift factor, a_T, which is, within experimental uncertainties, the same as the shift factor obtained from rheological data. When rheological properties are determined through the variations of the complex shear moduli G', G'' as a function of frequency, ω, one may superimpose the data obtained at different temperatures using a horizontal shift factor. This shift factor a_T will be the same in a peeling experiment when the peeling force (F) is plotted as a function of peeling rate (V). This rather "old" experimental fact [2] is nevertheless an extraordinary feature, as it is observed also at high peeling rates where fracture is interfacial, in a domain where viscoelastic properties should play a minor role as opposed to cohesive fracture: the peeling curve being a "rheological curve" in the whole range of peeling rates, rheology should be the dominant feature for all fracture modes.

The mode of fracture observed in a peeling experiment depends on (i) the adhesive/substrate interface, (ii) the peeling rate and/or (iii) the temperature. When the sample is of the flexible substrate/adhesive/rigid substrate type, one may observe two modes of fracture:

- cohesive fracture: the crack propagates within the adhesive. One may observe after the experiment an adhesive layer on each side of the sample probe.
- interfacial fracture: the crack propagates at the interface between one substrate and the adhesive. Two different modes may be observed depending on the crack location (flexible or rigid substrate).

These general features may differ, however, from one formulation to another. One may observe: transitions with a change in fracture location along with – or without – a drop in the peeling force; transitions

with a drop of the peeling force but without any change in location of the fracture [3]. So, if peeling curves may be considered as rheological curves, rheology is certainly not the whole story in the interfacial fracture domain.

The present paper presents a detailed study of the **cohesive fracture** domain in the case of structurally and rheologically well-defined adhesives.

We will first demonstrate that the peeling master curves are not dependent on experimental artifacts (location of crack initiation); then we will analyze the cohesive domain and relate the peeling behaviour to the rheological properties which are directly governed by the polymer molecular weight, resin volume fraction and temperature. Furthermore, we will study the effect of the mechanical behavior of the adhesive on peel geometry, which has been checked for all the experiments using a videocamera.

This paper, which deals mainly with cohesive fracture at low and moderate peeling rates, is the first of a series in which we will subsequently study the other peeling domains (interfacial-rubbery/stick-slip, then stick-slip/interfacial-glassy) and relate the adhesion properties to the rheological and interfacial properties of well-defined adhesives.

1. EXPERIMENTAL

1.1. Samples

Commercial hot-melt and pressure sensitive adhesives are made of elaborate formulations; the main components are generally a polymer which gives resistance to the adhesive as well as high viscous losses during a fracture process, and a tackifying resin which gives "tack" during the process. The relationship between the adhesive properties and the composition of these materials is described in the literature in very general and qualitative terms, and the formulations of hot-melts and pressure-sensitive adhesives (PSA) proceeds mainly from rules of thumb and/or trial-and-error methods. In order to quantify the relationship between the rheological properties, adhesive properties and the composition of adhesive formulations, we have studied well-defined formulations in the present series of papers: the basic polymers are quasi-monodisperse anionic polybutadiene samples which have been synthetized by the Michelin Company (France); the tackifying

resin was a terpene-phenolic resin (Dertophene T) from the D.R.T. Company (France). This resin is an unentangled oligomer which has a double effect: a "topological" effect which swells the entanglement network of the polymer and a thermodynamic effect which increases the glass transition temperature of the formulation (antiplasticizing effect) [4].

The blends were made by dissolving the polymer and the resin in benzene, the solution being agitated during 24 hours; then the solvent was removed by freeze-drying during 5 days. The molecular weight, polydispersity values and glass transition temperatures (obtained by dynamic mechanical analysis) of the samples are reported in Table I.

A series of blends were made using the two basic linear polymers (PB1 and PB2). The blends are referenced in the following way: the first two digits indicate the polymer volume fraction (25 = 25%), the last two digits indicating the resin volume fraction; the polymer is identified as PB1 or PB2 between these two numbers (example: 30PB170).

1.2. Rheological Experiments

Rheological characterization of our adhesives has been made by measuring the complex shear modulus (G', G'') as a function of frequency, ω, at various temperatures. These mechanical spectroscopy experiments [5] have been performed in the frequency range 10^{-2}–500 rad s^{-1} using a Rheometrics RDA700 rotational rheometer in parallel-plate geometry. The use of the time-temperature superposition principle allows one to plot master curves which feature the main relaxation domains, from the terminal relaxation region (flow region) up to the glassy behavior (T_α relaxation) at high frequencies.

TABLE I Glass transition temperatures (TMA) and molecular weights (GPC) of the basic polymers

	PB1	*PB2*
Structure	11% 1–2 48% trans	11% 1–2 48% trans
Weight average molecular weight ($g.mol^{-1}$) Mw	150 000	65 000
Glass transition temperature (°C) Tg	−88	−88
Polydispersity index	1.09	1.05

We have also performed thermomechanical experiments, following the variation of G' and G' at a fixed frequency (10 rad/s) in the temperature range -120 to 100°C.

The platen diameter was varied from 5 mm to 25 mm, depending on the modulus level, in order to minimize instrument compliance and sample slip effects.

We will deal in this paper only with the dynamic shearing behavior in the terminal and plateau regions which is relevant to cohesive fracture and the data obtained at higher frequencies will be presented in papers to follow. The thermomechanical analysis data will be presented in the whole temperature range in order to illustrate the various types of behavior relevant to the processing and final properties of the adhesive.

1.3. Peeling Experiments

They were performed on an Adamel Lhomargy DY 30 tensile machine which was equipped with an environmental chamber. We performed isothermal experiments, measuring the peeling force as a function of peeling rate at each temperature. The available peeling rate range was 1 to 1000 mm/min and temperature range -50 to 120°C, so we have been able to characterize all peeling modes for every formulation.

We have selected the ASTM D 3167-76 normalized peeling test, which is a "floating roller" test at constant peeling rate (Fig. 1). The peeling samples are sandwich-type "probes" made of three parts:

- a flexible aluminium substrate (thickness: 104 μm), which is often assumed to be non-extensible (the limits of this assumption will be discussed in section 4.3.1). The only surface treatment of that substrate was a thorough cleaning with acetone.
- a rigid aluminium substrate (thickness: 2 mm). In order to control its surface quality, the rigid aluminium substrate was sanded in a controlled way.
- the adhesive itself was pressed between the aluminium substrates in several steps and at elevated temperature (80°C) in order to reach a standard gap of 130 μm.

Each probe was carefully prepared and the adhesive thickness was controlled using an electronic micrometer. The uncertainty in adhesive thickness may be estimated to be 10%.

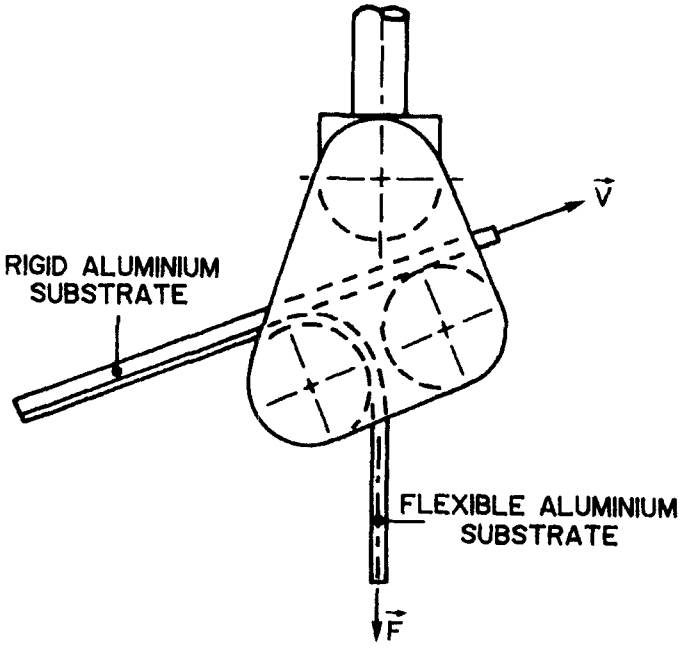

FIGURE 1 Principle of a floating-roller peeling experiment.

2. EXPERIMENTAL RESULTS: PEELING MASTER CURVES

We have performed peeling and rheological experiments on various (polymer + tackifying resin) blends, varying the volume fraction of both components. Before analyzing the adhesive properties of the formulations in the light of their rheological properties, the first question to answer is if the peeling curves (and *a fortiori* the master curves) are really free of artifacts and relevant to the adhesive properties themselves. We will demonstrate by two simple experiments the "objective" character of the peeling curves presented here.

The selected blend is 30PB170, which contains 30% polymer (volume fraction) and 70% resin.

2.1. Constructing Peeling Master Curves. The Shift Factors a_T

We have plotted on Figure 2 the variations of the peeling force as a function of peeling rate. We have used the data obtained at six

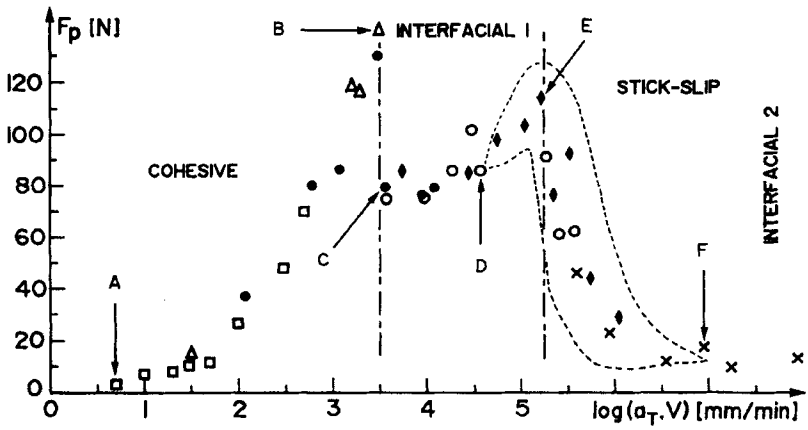

FIGURE 2 Peeling master curve for sample 30PB170: Peeling force as a function of peeling rate on a semi-logarithmic scale (reference temperature: $T_0 = 25°C$; □: 24°C ; ●: 15°C; △: 10°C; O : 5°C; ◆: 0°C; X : −10°C.

temperatures (−10, 0, 5, 10, 15, 25°C) to build this master curve at a reference temperature of 25°C, using a horizontal shift a_T. A slight vertical theoretical shifting, which lies within experimental uncertainties, has also been applied in order to take into account the thermal expansion of the adhesive: this vertical shift, b_T, which should be $\rho_0 T_0/\rho T$, is often approximated in the literature as T_0/T [1]. In the following sections, what we call F_p is the corrected peeling force $F_p = F T_0/T$. Figure 3 demonstrates that the shift factors used to construct the peeling master curves are, within experimental uncertainties, the same as the rheological shift factors.

We can observe that for this formulation the transitions between the various peeling domains are well marked. We can identify on this master curves the various types of fracture encountered when one wishes to separate two surfaces linked together by a viscoelastic adhesive, whatever the adhesion test. We can observe three stable fracture modes:

- cohesive fracture (from A to B).
- interfacial fracture mode 1 (from C to E). The adhesive remains on the flexible aluminium side. Starting from point D, one may observe a slight instability with no observable effect on the force level.
- interfacial fracture mode 2 (starting from F). The adhesive remains on the rigid aluminium substrate.

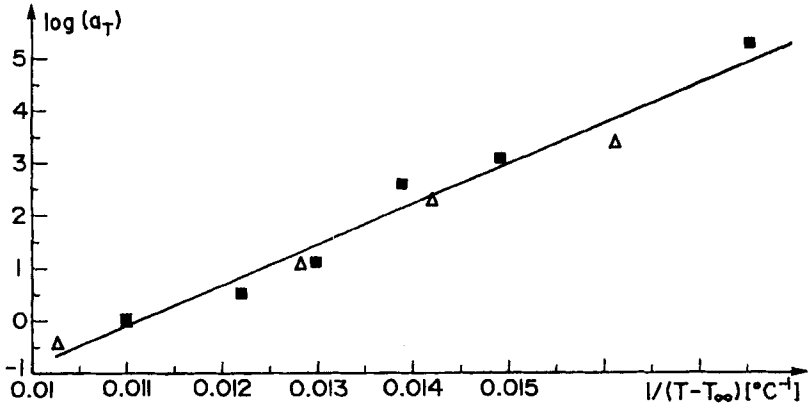

FIGURE 3 Comparison of time-temperature shift factors derived from peeling and rheological measurements (reference temperature $T_0 = 25°C$; △: a_T rheology; : ■: a_T peeling).

Starting from point E, there is an instable fracture mode ("stick-slip") which ends at point F. During the stick-slip, the adhesive remains on the rigid substrate. The recording of the peeling force presents oscillations of small period but large amplitude. The points plotted on Figure 2 correspond, in the stick-slip region, to averages between the maxima and minima of the force amplitude.

We have also shown that this peeling master curve, which presents various fracture modes as a function of temperature and/or peeling rate, is free of any experimental artifact and is reproducible whatever the experimental procedure: this is what we call the "objectivity" of this curve; in particular, crack propagation does not depend on the preparation and setting of the probe. Two simple experiments demonstrate that fracture location during a peeling test does not depend on the way it has been initiated: for a given substrate, it depends only on the rheological properties of the polymer at the temperature considered.

During the setting up of the probe before a peeling test, it is necessary to peel the flexible substrate manually before putting it in the machine clamp. During this setting-up procedure, crack initiation may occur within the adhesive or at either interface. The two experiments we have performed demonstrate that the location of crack initiation does not affect the peeling curve and that the crack location at a given peeling rate is always reproducible and independent of the way it was initiated.

2.2. Objectivity of the Peeling Master Curves

If we put a coating of silicone oil on the rigid aluminium substrate before we deposit the adhesive, we direct the adhesive to remain on the flexible adhesive side during a peeling test, whatever the peeling rate and temperature. We have coated the first part of a probe on the rigid aluminium side with silicone oil, which implies crack initiation on the rigid aluminium interface at the beginning of the experiment. If we are in experimental (peeling rate/temperature) conditions so that peeling occurs ususally at the flexible aluminium interface, we have observed that failure returns again at the flexible aluminium interface once the part coated by silicone has been peeled.

A similar experiment has been performed which consists in changing the temperature during a peeling experiment. We have first peeled the first part of the probe at temperature and peeling rate conditions such that peeling occurs at the rigid aluminium interface. We stop then the experiment and set a new temperature corresponding to a failure on the opposite side: after stabilisation of the temperature, we have observed that peeling always returns to its "natural" side (here the flexible aluminium side). Figure 4 is a photograph of the probe after such an experiment. We have observed the same features upon changing peeling rate instead of temperature; inverting the order of the fracture modes leads also to the same conclusions.

These two simple experiments demonstrate that there is a "natural" configuration of less energy the system will undertake whatever the fracture mode. This configuration depends on the adhesive/adherend interface and on the rheological behavior of the adhesive at the temperature considered. These experiments demonstrate that fracture is governed only by the adhesive properties for a given test geometry, the same way as the rheological properties govern the peeling curves whatever the fracture mode (same temperature shift factors). This is a very important result for industrial applications: the fact that fracture does not depend fundamentally on the location of crack initiation means that within a controlled range of temperature and deformation rates, the user may "trust" the adhesive even when some defect initiates a crack in a fracture mode which is different from what is expected.

Starting from the general description of the peeling behavior of adhesives described above, we have studied in detail each domain of

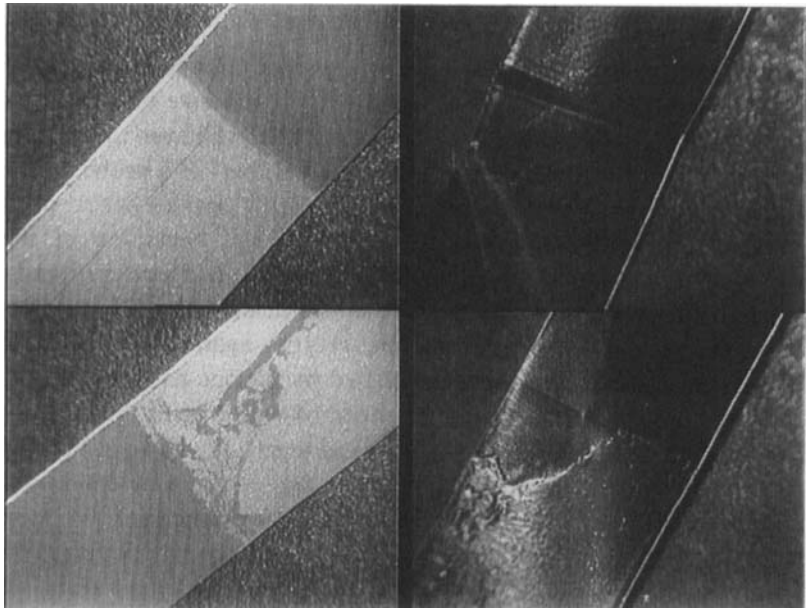

FIGURE 4 Change in fracture location upon changing peeling rate. (See Color Plate I).

the master peeling curves as a function of composition of our model adhesives. This first paper is relevant to the first domain: cohesive fracture.

3. EXPERIMENTAL RESULTS: RHEOLOGICAL PROPERTIES IN THE TERMINAL REGION AND COHESIVE FRACTURE

3.1. Viscoelastic Properties in the Terminal and Plateau Regions

We have measured the rheological properties of all blends following the method described in the first section. We have reported on Figures 5 and 6 the variations of the complex shear modulus $G^* = G' + jG''$ as a function of circular frequency, ω, for two formulations: 30PB170 and 30PB270. There are three important rheological parameters in the terminal region of relaxation (lowest frequencies):

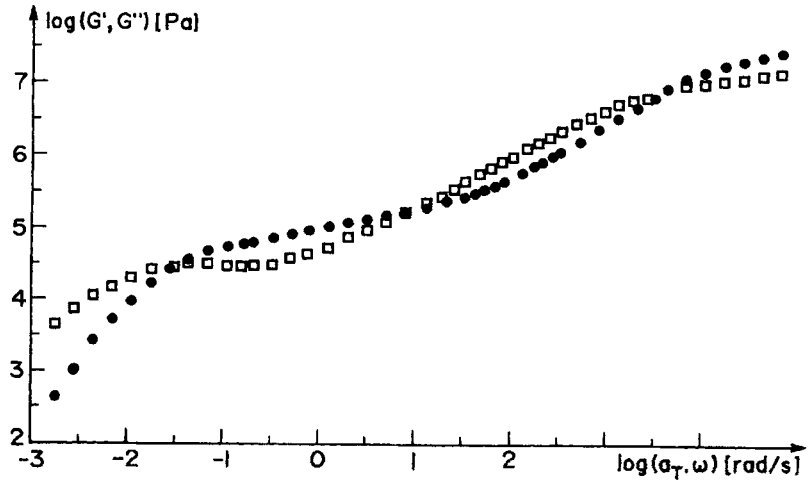

FIGURE 5 Master curve of mechanical spectroscopy for sample 30PB170: storage (●: G′) and loss (□: G″) moduli as a function of frequency (reference temperature $T_0 = 25°C$).

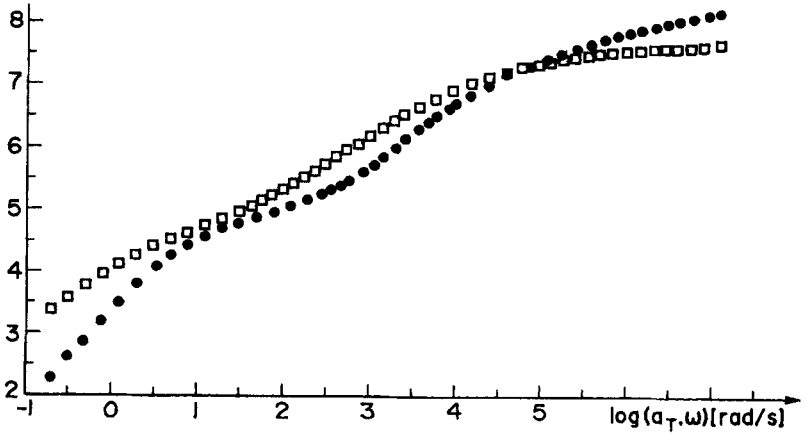

FIGURE 6 Master curve of mechanical spectroscopy for sample 30PB270: Storage (●: G′) and loss (□: G″) moduli as a function of frequency (reference temperature $T_0 = 25°C$).

– the zero-shear viscosity

$$\eta_0 = \lim_{\omega \to 0} \frac{G''(\omega)}{\omega}$$

– the recoverable compliance

$$J_e^0 = \lim_{\omega \to 0} \frac{G''(\omega)}{[G''(\omega)]^2} = \frac{1}{\eta_0^2} \lim_{\omega \to 0} \frac{G''(\omega)}{\omega^2}$$

– the terminal relaxation time

$$\tau_0 = \eta_o J_e^0$$

At intermediate frequencies, G' exhibits a "plateau" domain: $G' \approx G_N^0$. All these features are now well-known and well-defined in terms of structure/viscoelastic properties relationships [4].

One may observe that the addition of 30% resin makes the rubbery plateau region disappear for the polymer of lowest molecular weight, PB2; the strong implications of this feature on interfacial fracture will be analysed in a subsequent paper. Figure 7 presents the thermomechanical analyses of 2 samples: the bulk polymer PB2 and formulation 30PB270: resin addition creates a large increase of the glass transition temperature as well as a strong narrowing of the rubbery plateau domain. The variations of the plateau modulus, G_N^0, and limiting compliance, J_e^0, as a function of polymer volume fraction are

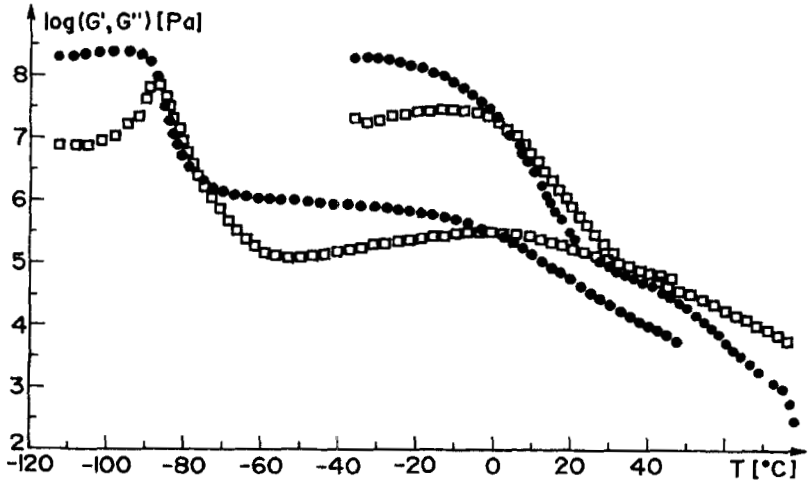

FIGURE 7 Thermomechanical Analysis curve for formulation 30PB270 compared with the bulk polymer PB2.

plotted on Figure 8. The power law variations observed:

$$(G_N^0)_{\text{blend}} = \Phi^{2.25}(G_N^0)_{\text{polymer}} \text{ and } (J_e^0)_{\text{blend}} = \Phi^{-2.27}(J_e^0)_{\text{polymer}}$$

indicate compatibility of the resin with polybutadiene; another (less precise) argument for compatibility is the observation of a single glass transition temperature on the thermomechanical analysis curves. A detailed analysis of these arguments as well as the general features of the viscoelastic properties of hot-melt adhesives have been given earlier [4, 6, 7].

The analysis of the viscoelastic properties show that the viscosity at 25°C of the adhesive formulation is higher than the viscosity of the bulk polymer up to a resin content of 80%. At higher values of resin volume fraction, the effect is reversed: the viscosity of the blend is lower than the viscosity of the bulk polymer. This is due to the fact that at low and moderate resin content, the antiplasticizing effect of the resin which increases the glass transition temperature of the blend overcomes the topological effect which increases the molecular weight between entanglements and should lower the viscosity. The viscosity may be written as [4, 7]:

$$\eta_0 \propto (\phi M)^{3.4} \exp\left(-\frac{B}{T - T_\infty}\right)$$

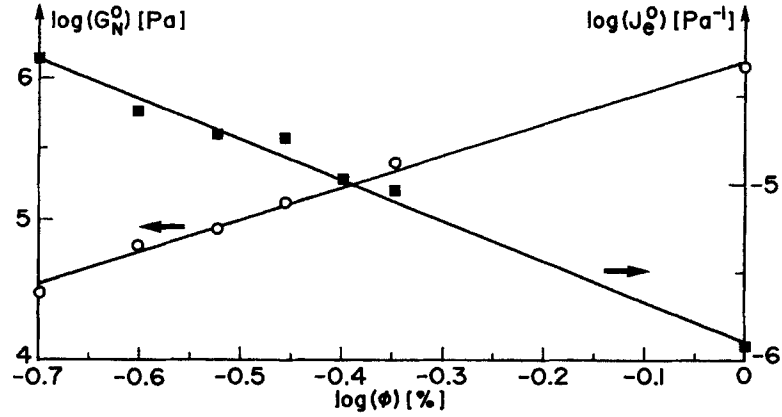

FIGURE 8 Variations of the plateau modulus and limiting compliance of the various formulations as a function of polymer volume fraction. ○: G_N^0; ■: J_e^0.

where the first term $(\phi M)^{3.4}$ represents the topological effect of polymer dilution, whereas the second term $\exp(-B/T-T_\infty)$ represents the mobility factor depending mainly on the glass transition temperature of the blend [7]. The relation $T_g - T_\infty \approx 60°C$ which was found to be a good approximation for concentrated polymer solutions applies also here. The terminal (reptation) time is the product $\tau_0 = \eta_0 J_e^0$ [4].

All these important rheological parameters have been reported in Table II.

As we know the temperature, molecular weight and concentration dependence of viscosities and relaxation times, we can calculate the various viscosity and relaxation time changes (*i.e.* the shift factors) upon changing the formulation and/or temperature. Furthermore, as the components of the formulations are structurally well defined, we are able to calculate the linear viscoelastic behavior (hence G' and G'' as a function of ω or T) with a good accuracy using models of molecular dynamics [8].

3.2. Cohesive Fracture

We have reported on Figure 9 the peeling data (peeling force *vs* peeling rate) obtained for the various formulations; the reference temperature is 25°C and, as stated above,the adhesive thickness is the same for all samples (130 μm). The first observation is that the peeling force increases first as the polymer volume fraction decreases; that effect is reversed when polymer volume fraction is lower than 25%. If one uses a double logarithmic plot (lower curve in Fig. 9), the experimental points follow approximately a power-law with the same slope (≈ 0.6) for all samples, as already shown for rubbery adhesives [9, 10, 11].

3.3. Phenomenological Analysis

In order to correlate the viscoelastic properties with the peeling data, we have first tried to build a peeling master curve for all formulations using a rheological reducing parameter in the peeling rate scale. The starting idea was to build a master curve which would be independent of the composition of the formulation: it has already been shown that, as far as rheology is concerned, the viscoelastic properties in the terminal region of relaxation may be described by a master curve inde-

TABLE II Rheological parameters of the bulk polymers and various formulations

	RHEOLOGICAL PARAMETERS								
	20PB180	25PB175	30PB170	35PB165	40PB160	45PB155	PB1	30PB170	PB2
Log (ϕ)	−0.699	−0.602	−0.523	−0.456	−0.398	−0.347	0	−0.523	0
η_0 (Pa.s)	$4.92\ 10^3$	$5.56\ 10^6$	$2.78\ 10^6$	$8.00\ 10^5$	$3.26\ 10^5$	$9.69\ 10^4$	$1.18\ 10^5$	$1.09\ 10^4$	$5.62\ 10^3$
τ_0 (min)	$4.20\ 10^{-3}$	2.38	0.88	0.25	$5.8\ 10^{-2}$	$2\ 10^{-2}$	$2.4\ 10^{-3}$	$5.7\ 10^{-3}$	$2.21\ 10^{-4}$
G_N° (Pa)	$3.00\ 10^4$	$6.40\ 10^4$	$8.46\ 10^4$	$1.30\ 10^5$	$2.00\ 10^5$	$2.50\ 10^5$	$1.20\ 10^6$	$8.46\ 10^4$	$1.20\ 10^6$
J_e° (Pa^{-1})	$5.12\ 10^{-5}$	$2.57\ 10^5$	$1.89\ 10^{-5}$	$1.80\ 10^{-5}$	$1.07\ 10^{-5}$	$9.21\ 10^{-6}$	$1.20\ 10^{-6}$	$3.16\ 10^{-5}$	$2.37\ 10^{-6}$

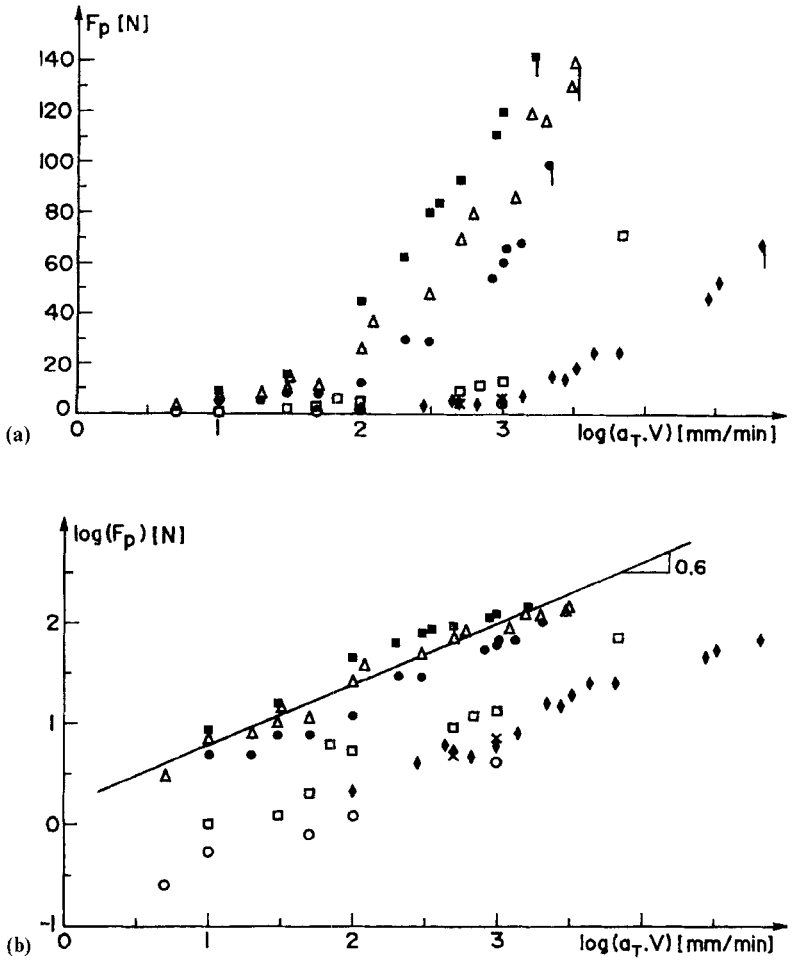

FIGURE 9 Peeling force as a function of peeling rate on a semi-logarithmic (a) and double-logarithmic (b) scale in the cohesive fracture domain. Master curve at 25°C for samples: O: 20PB180; ▲: 45PB155; □: 40PB160; ●: 35PB165; △: 30PB170; ■: 25PB175; ◆ : 30PB270.

pendent of molecular weight and polymer volume fraction. That is, time-temperature equivalence may be extended to time-molecular weight and time-concentration equivalence [12]. Hence, the terminal relaxation time, τ_0, is also a reducing parameter for the peeling curves: we have reported on Figure 10 the reduced peeling curves as the

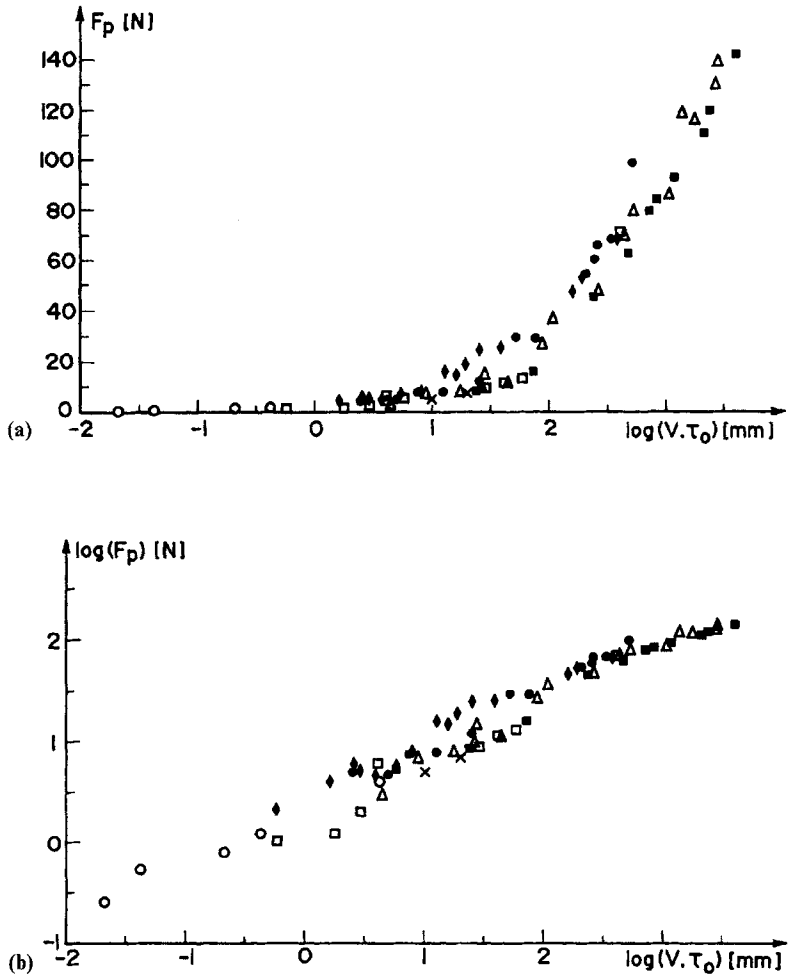

FIGURE 10 Peeling force as a function of reduced peeling rate ($V\tau_0$) on a semi-logarithmic (a) and double-logarithmic (b) scale in the cohesive fracture domain. Master curve at 25°C for samples: O: 20PB180; ▲: 45PB155; □: 40PB160; ●: 35PB165; △: 30PB170: ■: 25PB175; ◆: 30PB270.

peeling force, F_p, as a function of reduced peeling rate, $V \cdot \tau_0$. The double logarithmic plot yields also a line of slope 0.6. This important result shows that the reptation time is the characteristic time governing peeling in the cohesive fracture domain: this is also a fundamental design tool already used to design commercial formulations.

If we refer to the "trumpet" model of de Gennes [13], the crack length is related to the product $V \cdot \tau_0$. This model, designed for a simple viscoelastic solid, may not be simply and directly applied to our case which deals with a viscoelastic liquid with two main relaxation domains; qualitatively, however, our formulations exhibit the various transitions described by de Gennes' model.

The fact that there is no translation on the vertical (force or energy) axis shows that the mechanical behavior of the adhesive is the same at the same value of the reduced rate $V \cdot \tau_0$. A close observation of the peeling geometry shows a decrease of the radius of curvature of the flexible aluminium substrate when the peeling rate increases, the aluminium substrate leaving the roller even at moderate peeling rates. We will analyse in detail that effect in the following section. We will conclude the present section by stressing how important is the result of getting a peeling master curve as far as formulation design is concerned. Such a curve leads to a predictive tool for solving problems linked to the processing as well as final properties of adhesives. For example, the terminal relaxation time is very sensitive to polymer polydispersity, whereas its viscosity depends mainly on the weight-average molcular weight [14]: it is then possible to "play" with both parameters to improve formulation design.

4. GEOMETRY CHANGES DURING A PEELING TEST

In the floating-rollers peel tests, as well as in other peel tests, the test geometry changes with peeling rate: in our case, the flexible aluminium foil does not follow the radius imposed by the roller, even at moderate peeling rates. We have studied in detailed that effect (see schematic on Fig. 11).

4.1. Variations of the Radius of Curvature of the Flexible Aluminium with Peeling Rate: Detailed Study with Sample 30PB270

We have made a video recording of each peeling experiment and measured the radius of curvature, R_c, of the flexible aluminium substrate at each peeling rate. These data have been reported on Figure 12: the radius R_c decreases steadily with peeling rate and that effect on the measured force may not be neglected.

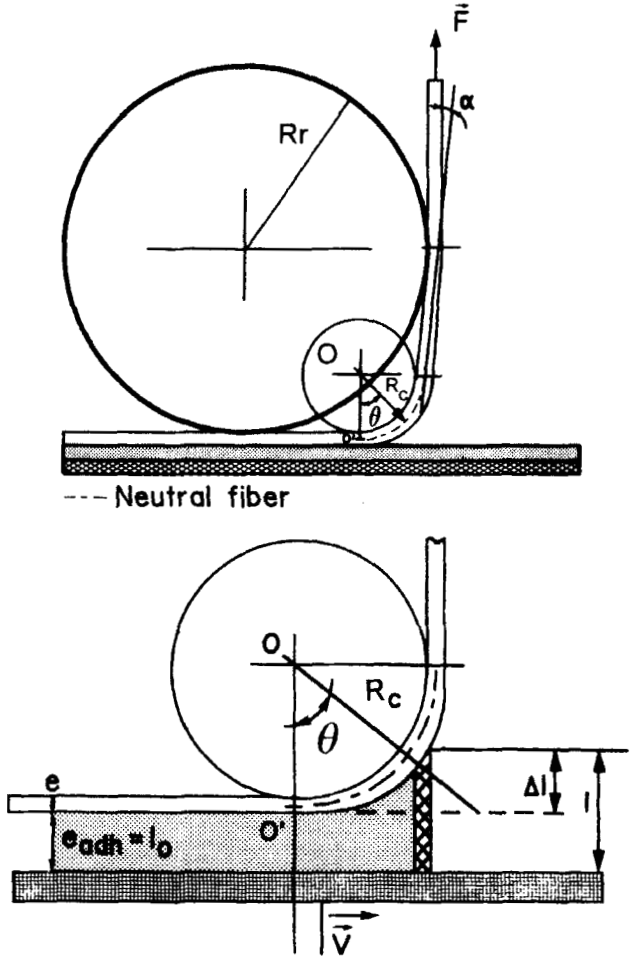

FIGURE 11 Schematic of deformation of the flexible aluminium foil and adhesive in the cohesive fracture region at intermediate peeling rates.

When the adhesive is deformed at low peeling rates, there is simply a flow of the adhesive (simple reptation of the polymeric chains) and the flexible aluminium follows the roller. At higher rates the adhesive becomes elastic and its relaxation time will govern its deformation: in that case, the adhesive will impose, in fact, the radius of curvature of the substrate. The variations of the radius of curvature (Fig. 12) may be

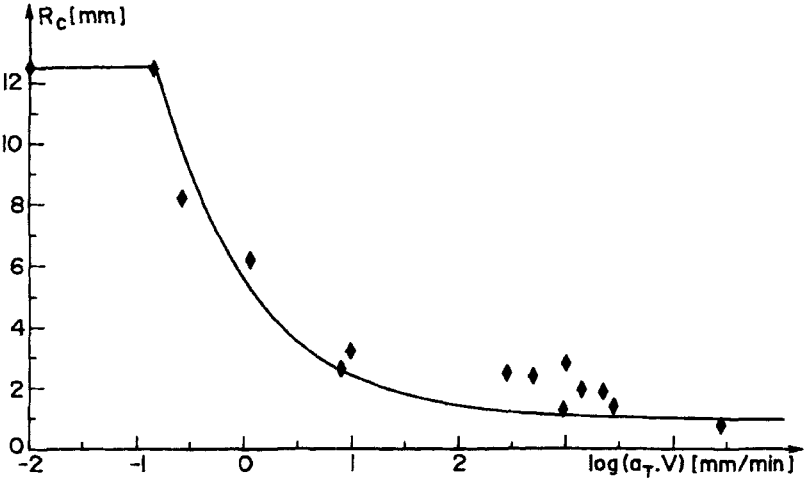

FIGURE 12 Variations of the radius of curvature as a function of peeling rate for sample 30PB270 (reference temperature $T_0 = 25°C$).

fitted by a power law:

$$R_c = k\ V^{-0.5} + R_0 \tag{1}$$

There is a rapid decrease of the radius, R_c, as a function of peeling rate down to a limiting value R_0. That limiting value depends only on the nature and thickness of the flexible substrate: we enter then a third domain where the test geometry is imposed by the flexible substrate.

The above phenomenological description implies that one may divide the peeling force F into two components:

$$F_p = F(\text{bending}) + F(\text{adhesive})$$

At low peeling rates, the two contributions are small, hence we measure low values of the peeling force. At moderate peeling rates, there is a strong increase of the peeling force with a strong decrease of the radius R_c: there is a large increase of the two terms of the above equation due to a large contribution of the bending moment of the aluminium to the overall force and a strong "hardening" of the adhesive. The limiting radius, R_0, has already been reached when the fracture mode changes from cohesive to interfacial.

The level of peeling forces in the interfacial/glassy domain is much smaller than in the cohesive domain; the radius R_c is, however, much smaller, and the contribution to the peeling force of the adhesive, which behaves as a glass in that domain, should also be small. This implies that a strong plastic deformation of the aluminium occurs in that domain, otherwise the large values of the bending moment due to the small values of R_c should lead to large values of F(bending), hence large values of F_p, which are not observed experimentally. The calculations presented in section 4.3 will justify that argument.

Kinloch and Williams [15,16] have recently presented a theoretical calculation of the contribution of the flexible substrate to the overall force for a 180° peeling test. This calculation, which is based on the measure of the real angle between the rigid substrate and the flexible substrate, leads to the adherence energy of the adhesive. Despite the difficulty of measuring the real angles, the calculation seems in good agreement with the experimental data. We do think also that a fine study of the test geometry is absolutely necessary if one wishes to model the peeling behavior in a wide range of peeling rates. So the analysis of the present work begins with a detailed description of the test geometry effects, in order to eliminate adjustable parameters introduced, for example by Gent and Petrich [17] or Connely *et al.* [18].

4.2. A Master Curve for the Variations of R_c

The evidence that it is really the adhesive which imposes the radius of curvature is that the variation of R_c as a function of peeling rate is also a "rheological curve": the relaxation time, τ_0, is also a reducing parameter in the peeling rate scale, and the $R_c(V\tau_0)$ curve (Fig. 13) is a master curve for all formulations.

The uncertainty in the given values of the radius of curvature increases as the radius becomes smaller: whereas the given values of R_c are determined with a reasonable accuracy in the decreasing region, the uncertainty is large in the value of the limiting radius R_0 ($R_0 < 1$ mm). In the following sections, the variations of the radius R_c with peeling rate will be represented by the reduced law:

$$R_c = k\,(V\tau_0)^{-0.5} + R_0 \tag{2}$$

with $k = 0.4$.

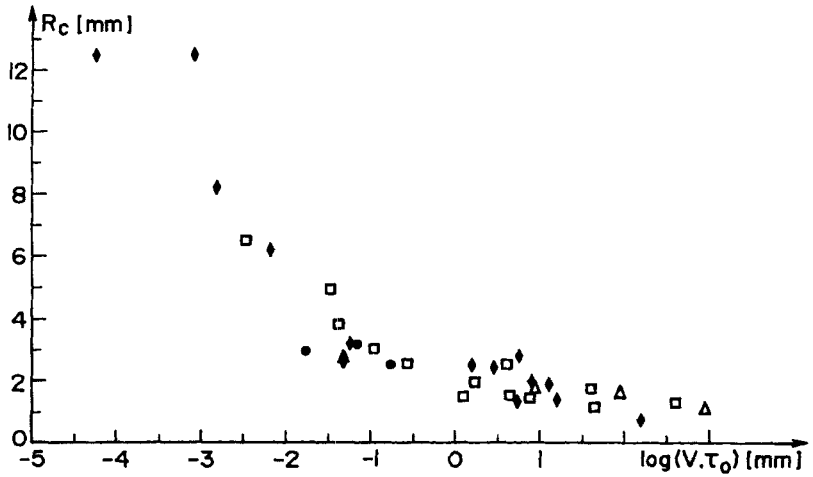

FIGURE 13 Variations of the radius of curvature as a function of reduced peeling rate ($V\tau_0$) (same samples as in Fig. 10).

4.3. Theoretical Analysis of Geometry Changes with Peeling Rate

4.3.1. Description of the Moments Applied to the System; The Effects of Plastic Deformation of the Aluminium Substrate

Let us define an open system, S, as the bent part of the flexible aluminium foil. We may use the angular moment law which states that the sum of moments of forces exerted on the system may be written as:

$$\frac{d\vec{\sigma}_0}{dt} = \vec{V}(O) \wedge m\vec{V}(G) + q_m(O\vec{O}' \wedge \vec{V}(O') - O\vec{M} \wedge \vec{V}(M))$$

$$= \sum \vec{M}_{/0}(\vec{F}_{ext}) \tag{3}$$

where $\vec{\sigma}_0$ is the angular moment of the aluminium foil, $\vec{V}(O)$ is the velocity of point O, $\vec{V}(G)$ the velocity of the centre of gravity of the bent part of the aluminium foil, and q_m the mass flow through the system S (see Fig. 14 where the system is described).

The velocity is 0 at point O. A peeling test is performed at constant peeling rate so we are in stationary conditions. The system is equivalent to a system at equilibrium, so:

$d\vec{\sigma}_0/dt = \vec{0}$; furthermore, the last term of the left hand side of Eq. (3) is also 0 in stationary conditions:

$q_m\left(O\vec{O'} \wedge \vec{V}(O') - O\vec{M} \wedge \vec{V}(M)\right) = \vec{0}$, hence we get at time t:

$$\sum \vec{M}_{/0}(\vec{F}_{ext}) = \vec{0} \tag{4}$$

This law applies only when there is no energy source or hole in the system, so it may not be used in the case of plastic deformation.

The various forces acting on the flexible substrate are indicated on Figure 14. Before analysing the effects of these forces in terms of their moments, we have to make some hypotheses:

- The moment created by the weight of the isolated curved part of the aluminium is negligible.

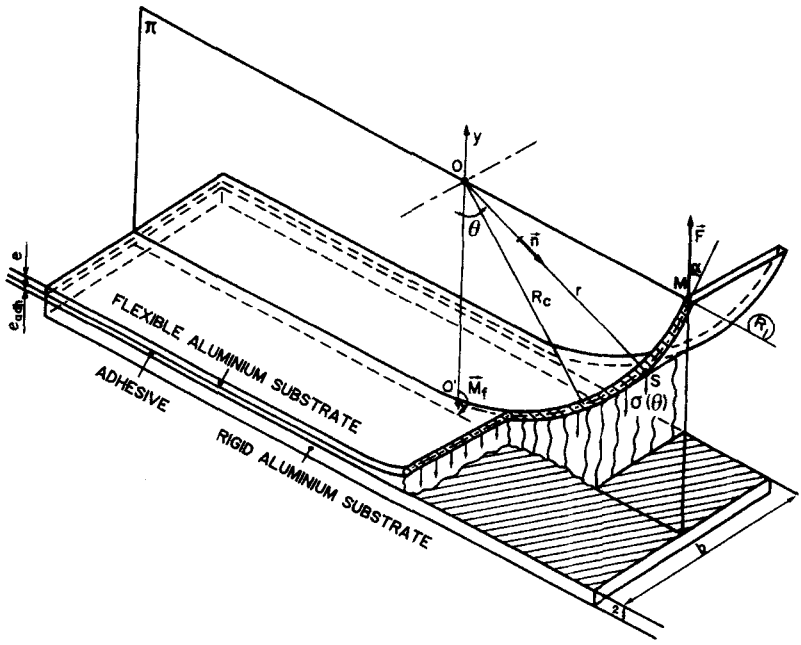

FIGURE 14 Schematic of the "System" S.

- We assume that the aluminium foil is linked to point O' which is a fixed point in a coordinate system linked to the aluminium foil.
- There is no sliding between the flexible aluminium and the mobile roller.

Remark: With respect to a Galilean laboratory coordinate system (R), the chosen coordinate system linked to the rigid aluminium substrate (R') has a uniform rectilinear translation motion and is also Galilean. One may apply then the fundamental laws of solid dynamics with respect to system R'.

Let us consider a point M belonging to the trace of the neutral fiber in plane (Π), which is the vertical plane of symmetry of the system. M is the application point of the force $\vec{F}$ and its angular position is given by the angle θ_M. All the forces and stresses generated are located in plane (Π). In a linear (elastic) behaviour domain, the balance of moments applied to the system is:

$$\vec{M}_{/0}(\vec{F}) + \vec{M}_f + \int_0^{\theta_M} \vec{M}_{/0}(\vec{\sigma}(\theta)\, dS)\, d\theta + \vec{M}_{/0}(\vec{N}) + \vec{M}_{/0}(\vec{T}) = \vec{0} \tag{5}$$

The three moments are, respectively, the moment with respect to O of the applied force $\vec{F}$: $\vec{M}_{/0}(\vec{F})$, the bending moment of the aluminium foil $\vec{M}_f$, the moment with respect to O of the stresses generated by the adhesive and the moment with respect to O of the shearing stresses. We are going to detail these three moments:

(i) the moment with respect to O of force $\vec{F}$ is $\vec{M}_{/0}(\vec{F}) = \vec{OM} \wedge \vec{F}$, and it can be expressed in our coordinate system (see Fig. 14) as:

$$\vec{M}_{/0}(\vec{F}) = (Fr_M \sin\theta_M \cos\alpha - Fr_M \cos\theta_M \sin\alpha)\, \vec{k} \tag{6}$$

where r_M is the radial coordinate of point M and $\vec{k}$ the unit vector in the direction perpendicular to plane (Π).

The angle α being small, $\cos\alpha \cong 1$ and the value of θ_M is 90° (see Fig. 14), so Eq.(6) becomes:

$$\vec{M}_{/0}(\vec{F}) = Fr_M \vec{k} \tag{7}$$

(ii) The elementary force induced by the stress field $\vec{\sigma}(\theta)$ is given by:

$$\vec{f} = \vec{\sigma}(\theta)\, ds = \vec{\sigma}(\theta) b\, r\, d\theta \tag{8}$$

assuming that the stresses $\vec{\sigma}(\theta)$ are uniform along the probe width, b. The moment with respect to O of this force will be:

$$\vec{M}_{/0}(\vec{f}) = \int_0^{\theta_M} d\vec{M}_{/0}(\vec{f}) = -b \int_0^{\theta_M} \vec{\sigma}(\theta) \wedge r^2\, \vec{n}\, d\theta \tag{9}$$

$\vec{n}$ being the unit vector in the $\vec{OS}$ direction (see Fig. 14).

(iii) The aluminium foil bending induces a moment with respect to point O. If the stresses $\vec{\sigma}'(z)$ are uniform along the width b, the bending moment is (Fig. 15):

$$\vec{M}_f = \vec{M}_{/0}(\vec{\sigma}'(z) ds') = \int_{s'} \vec{AP} \wedge \vec{\sigma}'(z)\, ds' = -b \int_{-e/2}^{e/2} \vec{\sigma}'(z) z\, dz\, \vec{k} \tag{10}$$

$ds' = b\, dz$ being the surface element.

(iv) The moment $\vec{M}_{/0}(\vec{N})$ of the normal forces at the entrance of the open system S (at point O') is:

$$\vec{M}_{/0}(\vec{N}) = \vec{OO'} \wedge \vec{N}$$

$\vec{N}$ is given by the kinetic moment equation:

$$\vec{N} = -q_m V \vec{i} \tag{11}$$

and

$$\vec{M}_{/0}(\vec{N}) = -q_m\, r_M V^2 \vec{k} = -\rho e b r_M V^2 \vec{k} \tag{12}$$

with $q_m = \rho e b V$, ρ being the aluminium density.

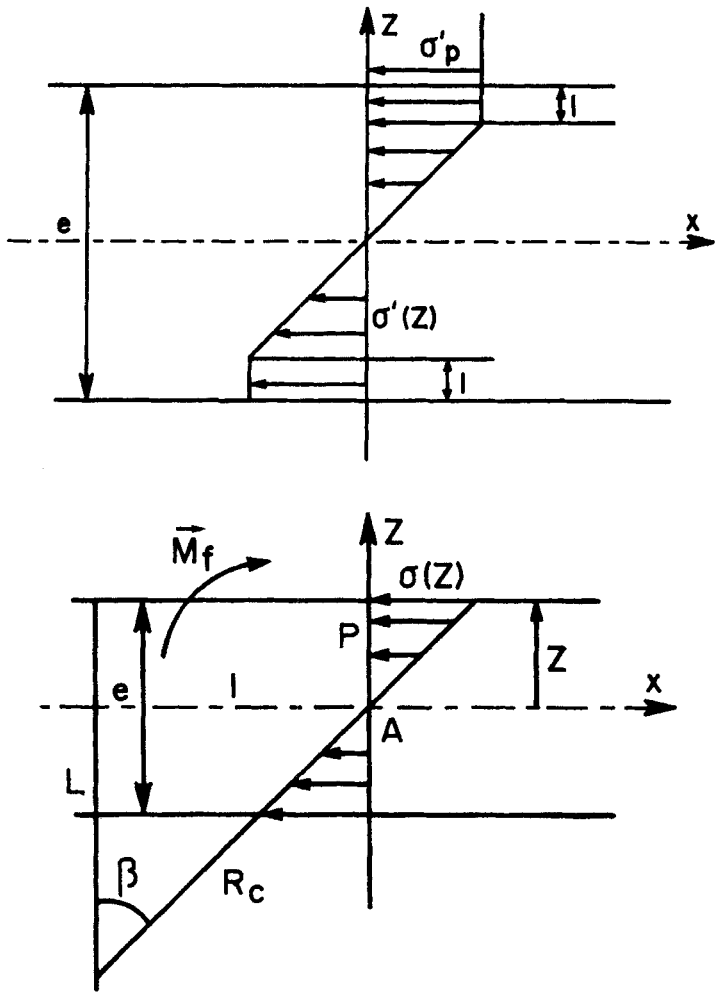

FIGURE 15 Schematic of stresses upon bending of the flexible substrate in two cases: (a) elastic deformation and (b) plastic deformation.

Equations (7), (9), (10) and (12) may then be introduced in the balance Eq. (5). We may then derive an expression for the force F as:

$$F = \frac{b}{r_M}\left[\int_{-e/2}^{e/2} \sigma'(z) z\, dz + \int_0^{\theta_M} (\vec{\sigma}(\theta) \wedge r^2\vec{n})\,\vec{k}\, d\theta + \rho e V^2\right] \qquad (13)$$

In the domain of peeling rates corresponding to cohesive fracture, the last term of Eq. (13) ($\rho e V^2$) is negligible [20], and this term will be neglected in the subsequent calculations.

We will simplify that equation assuming that the radius of curvature is constant and equal to the average radius of the neutral fibre, R_c, as indicated on Figure 11. Hence $r_M = R_c$ and $r = (R_c + e/2)$.

We assume that each volume element, dv, of the adhesive experiences an elongational deformation: hence, one neglects the shear deformation and the stresses are oriented in the y direction:

$$\vec{\sigma}(\theta) \wedge \vec{n} = \sigma(\theta) \sin\theta \, \vec{k}$$

and Eq.(11) becomes:

$$F = \frac{b}{r_M}\left[\int_{-e/2}^{e/2} \sigma'(z) z \, dz + \left(R_C + \frac{e}{2}\right)^2 \int_0^{e/2} \sigma(\theta) \sin\theta \, d\theta\right] \tag{14}$$

a) elastic deformation of the aluminium substrate:

Let us isolate the bent part of the aluminium foil. The deformation ε (see Fig. 15) is given by [19]:

$$\varepsilon = \frac{U}{R_C + U} = \frac{z}{R_C + z} \tag{15}$$

and in the case of purely elastic deformation:

$$\sigma'(z) = E\varepsilon = \frac{Ez}{R_C + z} \tag{16}$$

If we introduce that expression of $\sigma'(z)$ in Eqn. (14) and neglect the thickness, z, compared with the radius of curvature, R_C:

$$F = \frac{b}{R_C}\left[\frac{Ee^3}{12R_C} + \left(R_C + \frac{e}{2}\right)^2 \int_0^{\theta_M} \sigma(\theta) \sin\theta d\theta\right] \tag{17}$$

We retrieve the expression of the bending moment already given by Williams [15] in the case of a purely elastic deformation of the substrate (first term of right hand side of Eqn. (17)).

b) plastic deformation of the aluminum substrate:

It is possible to reach a state of plastic deformation of the flexible substrate at high peeling rates. Gent[21] has pointed out this effect and studied the plastic deformation of several substrates. We have demonstrated experimentally the plastic deformation of the flexible substrate [20] in the present case. If we go back to the expression for the bending moment, one may introduce a term of plastic deformation (Fig. 15):

$$M_f = \int_{1-e/2}^{e/2-1} \frac{bEz^2}{R_c}\,dz + 2\int_{e/2-1}^{e/2} \sigma'_p b z\,dz \tag{18}$$

where σ'_p is the plastic stress and l the plastically deformed thickness (Fig. 15).

In the case where the whole thickness experiences plastic deformation, the bending moment will be:

$$M_f = M_p = \frac{\sigma' be^2}{4} \tag{19}$$

and in the case of partial plastic deformation:

$$M_f = M_p\left[1 - \frac{(e-21)^2}{3e^2}\right] \tag{20}$$

If we define a parameter $x = R_c/R_r$. we recover the expression for the bending moment given by Williams [15]:

$$M_f = M_p\left(1 - \frac{x^2}{3}\right) \tag{21}$$

A comparison between the values calculated from Eqn. (19) and derived using the stress/strain experimental curve performed on the flexible aluminium substrate (Eq. (20)):

$$M_f = b\int_{e/2}^{e/2} \sigma(z) z\,dz \tag{22}$$

is given on Figure 16.

The plastic deformation induces heat dissipation, so we can no more use the kinetic moment law. We may, however, use the kinetic

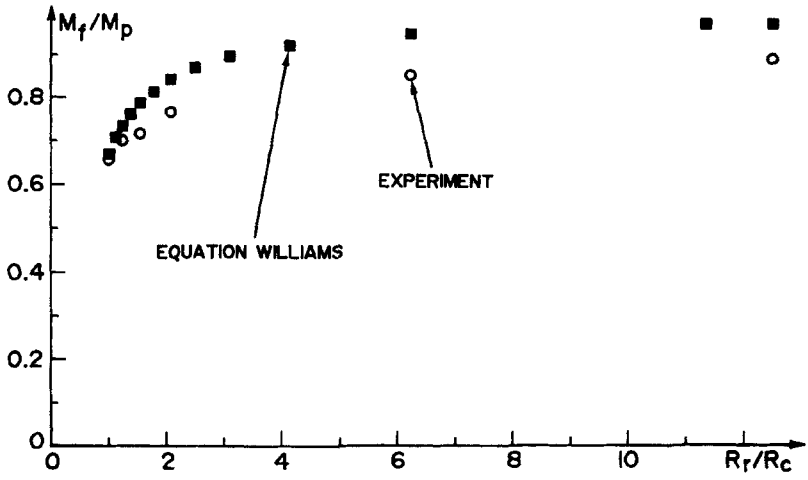

FIGURE 16 Variations of the ratio M_f/M_p as a function of reduced radius of curvature R_r/R_c; the theoretical values (■) have been calculated from the model of Willams [15], and the "experimental" (O) values derived from the experimental stress/strain curves (Eq. (20)).

energy law in order to derive a simple relation between the peeling force and the adhesive stresses, taking into account the dissipated energy:

$$P(\vec{F}_{ext}) + P(\vec{F}_{int}) = \frac{1}{2} q_m (V^2(O') - V^2(M)) \tag{23}$$

where S is the open system considered, R the laboratory system coordinate, $P(\vec{F}_{ext})$ the power of the external forces and $P(\vec{F}_{int})$ the power dissipated by the internal forces. The moduli of the velocity vectors at points O' and M being the same:

$$P(\vec{F}_{ext}) + P(\vec{F}_{int}) = 0 \tag{24}$$

As we are in stationary conditions, the angular rate of the system is constant; hence:

$$P(\vec{F}_{ext}) = \vec{\omega}_{S/R} \sum \vec{M}_{/O}(\vec{F}_{ext}) \tag{25}$$

So:

$$\sum M_{/O}(\vec{F}_{ext}) + \frac{P(\vec{F}_{int})}{\omega_{S/R}} = 0 \tag{26}$$

The dissipated work of plastic deformation per unit length in the bent part of the aluminium foil has been calculated by Williams [15]:

$$W = \frac{Ee^3 b}{8(R_r + e/2)^2}\left[\frac{1}{x} - \frac{7}{4} + \frac{x}{3} + \frac{x^3}{3} - \frac{x^4}{12}\right] \tag{27}$$

The work of inner forces may be written as a function of the power dissipated by these forces:

$$W_i = \int P(\vec{F}_{\text{int}})\, dt \tag{28}$$

W and W_i are related by:
$W_i/\Delta l = -W \Rightarrow -W\ \Delta l/\Delta t = P(\vec{F}_{\text{int}}) \Rightarrow -WV = P(\vec{F}_{\text{int}})$ where V is the peeling rate. Hence, one may compare the dissipated power with the overall power (FV). In the worst case, $x = 1/12.5$ because the maximum radius is the radius of the roller and the minimum measurable radius is of the order of 1 mm, so $W = 8$ J. This value may be compared with peeling forces measured at peeling rates where the radius of curvature is small: in that case, the peeling force is above 100 N, so the ratio W/F is of the order of 8%: the uncertainties in peeling measurements being large (15% in the peeling force alone), we may consider that the work of plastic deformation is negligible with respect to the peeling force.

At last, one may also calculate the contribution of the bending moment when one reaches small peeling radii. For a radius of 1 mm, plastic deformation may be considered as total, hence:

$$\frac{M_p}{R_C \sin\theta_M} \approx \frac{M_p}{R_C} = \frac{be^2\sigma_p}{4R_C} \approx 5\,\text{N}$$

This demonstrates that the overall peeling force is mainly due to the peeling of the adhesive itself even when there is a very large plastic deformation of the aluminium substrate at high peeling rates. As a consequence, Eq. (17) may be considered as the definite equation to calculate the peeling force: it includes a bending term if the deforma-

tion of the aluminium is elastic, the analytical form of the term due to the adhesive being always the same.

4.3.2. Calculation of the Overall Peeling Force. Comparison with Experiments

We have described the various contributions to the peeling force during a test performed at constant peeling rate. Equation (17) is then the definite equation in which we have to introduce the rheological behavior of the adhesive. We have used a non-linear integral constitutive equation of the KBKZ [22] type which describes fairly well the viscoelastic behavior of polymers in strong flows:

$$\sigma(t) = \int_{-\infty}^{t} m(t-t')\, h(\lambda)\, \tilde{C}_t^{-1}\, dt' \tag{29}$$

where $m(t)$ is the memory function derived from linear viscoelastic measurements, $h(\lambda)$ a damping function depending on the strain, λ, and $\tilde{C}_t^{-1}$ the Finger strain tensor. The memory function is related to the relaxation modulus by:

$$m(t) = -\frac{dG(t)}{dt} \tag{30}$$

The relaxation modulus $G(t)$ may be derived from the complex shear modulus $G^*(\omega)$ by an inverse Fourier transform. In our case, all these functions, derived from molecular models, are analytical [8]. For uniaxial deformation, the Finger deformation tensor is given by:

$$\tilde{C}_t^{-1} = \lambda^2 - \frac{1}{\lambda} \tag{31}$$

where λ is the local strain of the material during a peeling test.

Equation (29) contains an *ad hoc* function (the damping function, h) which corrects for the too-large strains predicted by the Lodge "elastic liquid" [23] constitutive equation ($h(\lambda) = 1$). The damping function we have used in our calculation has been given by Wagner [24] and fits

the non linear data in shear and elongation for a large number of linear polymers.

$$h(\lambda) = [\lambda^2 \exp(-m) + \lambda^a (1 - \exp(-m))]^{-1} \tag{32}$$

with $m = 4$ and $a = 0.3$.

From the standpoint of molecular models, the damping function is a universal function which does not depend on the molecular species considered, hence the universality of Eq. (26).

If we are able to define the state of strains within the system, Eq. (15) will allow us to calculate the peeling force at a given peeling rate. We give on Figure 11 a schematic of the deformation experienced by the adhesive upon peeling. The deformation of the adhesive is given by [25]:

$$\Delta l(R_C + e/2)(1 - \cos\theta) \tag{33}$$

where $l = e_{adh} + \Delta l$, and e_{adh} is the adhesive thickness.

If there is a no-slip condition between the flexible aluminium and the roller, the relation between the angular position, θ, and time, t, is:

$$\theta = \frac{Vt}{R_C} \tag{34}$$

where V is the peeling rate; hence, the corresponding Hencky strain rate:

$$\dot{\varepsilon} = \frac{1}{l}\frac{dl}{dt} = \frac{V \sin\theta}{e_{adh} + \Delta l} \tag{35}$$

and the Hencky strain:

$$\varepsilon = \int_{e_{adh}}^{l} \frac{dl}{l} = \ln\left(\frac{1}{e_{adh}}\right) = \ln\left(1 + \frac{R_C + e/2}{e_{adh}}(1 - \cos\theta)\right) \tag{36}$$

and the deformation rate, λ, appearing in the Finger tensor is:

$$\lambda = \exp(\varepsilon) \tag{37}$$

We have now all that we need to perform the calculation of the overall peeling force of Eq. (17), except the upper limit of the integral, which corresponds in fact to a fracture criterion. Our experience on the elongational properties of these materials is that at low and moderate strain rates, breaking occurs in uniaxial elongation at the same deformation, corresponding to 4.5 in Hencky strain. The link we establish here between peeling in the cohesive region and uniaxial elongation led us to select this criterion to define the upper limit of the integral; that is, the upper limit θ_M of Eq. (17) corresponds to a Hencky strain of 4.5. Otherwise, this angle is $\pi/2$ (which corresponds to the lowest peeling rates). A comparison between the experimental data and the above calculation is presented on Figure 17. The calculation allows to forecast reasonably well the peeling behavior in the cohesive domain. Furthermore, the viscoelastic behavior of the formulations which feeds the model may be calculated from the structural parameters (distribution of molecular weights, glass transition temperatures of the components and the composition of the blend (volume fraction of the components)), using molecular models [14]. This approach could indeed be a very useful predictive tool for adhesive formulation as there is no adjustable parameter in the calculation.

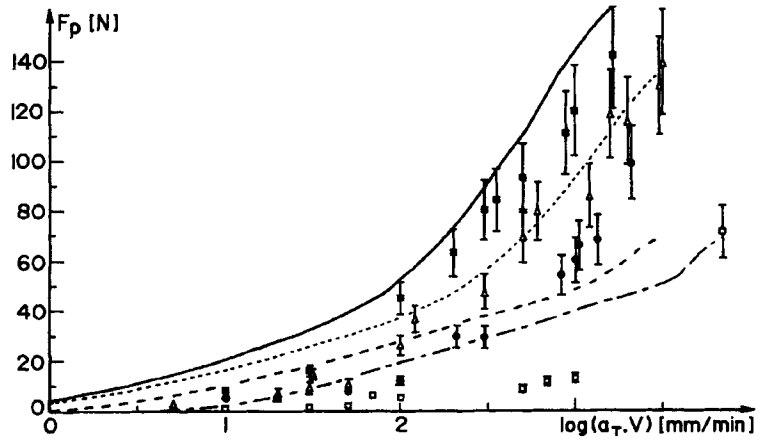

FIGURE 17 Comparison between the peeling force values calculated from the model (Eq. (12)):---:25PB175; ---: 30PB170;---:25PB165; --· — · —:40PB160) and the experimental data (same definition as in Fig. 9a; the error bars correspond to an uncertainty of 15%).

CONCLUSION

The viscoelastic and peeling properties of model hot-melt adhesives have been studied in a wide range of frequencies and peeling rates, using time-temperature equivalence. In the first paper of this series, we focus on the cohesive fracture domain, and we demonstrate that it is related to the viscoelastic terminal region of relaxation. One important result is that peeling curves obtained for different temperatures and/or adhesive formulations may be reduced to a single master curve: the reducing parameter in the peeling rate scale is the characteristic relaxation time τ_0, of the terminal region of relaxation: it accounts for the temperature dependence of the peeling curves (we recover time-temperature equivalence), but also for the effects of adhesive formulation: polymer molecular weight, resin content, glass transition temperature, etc. From a theoretical point of view, this result seems qualitatively in agreement with the "trumpet" concept of de Gennes; from a practical point of view, the use of this equivalence, which relates, quantitatively, cohesive fracture behavior with viscoelastic behavior, should be of great help in the design of adhesive formulations.

Our attempt to give a quantitative model of peeling behavior which takes into account the adhesive elongational properties, as well as the variations of peeling geometry, leads to a fracture criterion in the cohesive region which depends only on the overall elongational deformation of the adhesive. The model gives a reasonable agreement with the experimental data and accounts for the effects of temperature as well as adhesive formulation.

The papers to follow in this series will analyse the subsequent peeling domains (interfacial domain 1, stick slip, interfacial domain 2) in light of the viscoelastic behavior in the elastic plateau and glassy regions.

Acknowledgements

C. D., A. A. and G. M. thank the ElfAtochem company (Groupement de Recherches de Lacq) for financial support of this work. The Michelin Company is also gratefully acknowledged for the synthesis of the monodisperse polybutadiene samples.

References

[1] Ferry, J. D., *Viscoelastic Properties of Polymers*, 3rd ed. (J. Wiley, New York, 1970).
[2] Kaelble, D. H., *J. Coll. Sci.* **19**, 143 (1964).
[3] Wu, S., *Polymer Interface and Adhesion* (M. Dekker, New York, 1982).
[4] Marin, G., Menezes, E., Raju, V. R. and Graessley, W. W., *Reol. Acta.* **19** 462 (1980).
[5] Marin, G., *"Rheological Measurements"* in *Rheological Fundamentals of Polymer Processing* (Kluwer Academic, Dordrecht, 1995).
[6] Vandermaesen, Ph., Doctoral Thesis, Université de Pau (1992).
[7] Marin, G., Vandermaesen, Ph. and Komornicki, J., *J. Adhesion* **35**, 23 (1991).
[8] Benallal, A., Marin, G., Montfort, J. P. and Derail, C., *Macromolecules* **26**, 7229 (1993).
[9] Maugis, D., *J. Adh. Sci. Technol.* **1**(2), 105 (1987).
[10] Roberts, A.D., *Rubber Chem. Technol.* **52**, 23 (1979).
[11] Kendall, K., *J. Appl. Phys.* **6**, 1782 (1973).
[12] Marin, G., Montfort, J. P. and Monge, Ph., *Rheol. Acta* **21**, 449 (1982).
[13] de Gennes, P. G., *C. R. Académie des Sciences* **307** II, 1949 (1988).
[14] Marin, G. and Montfort, J. P., Chapter *"Molecular Rheology"* in *Rheology for Polymer Melts Processing* (Elsevier, New York, Amsterdam, 1996).
[15] Williams, J. G., *J. Adhesion* **41**, 225 (1993).
[16] Kinloch, A. J., Lau, C. C. and Williams, J. G., *Int. J. Fracture* **66**, 45 (1994).
[17] Gent, A. N. and Petrich, R. P., *Proc. Roy. Soc. London* **A300**, 433 (1969).
[18] Connelly, R. W. Parsons, W. F. and Pearson, G. H., *J. Rheol.* **25**, 315 (1983).
[19] Timoscenko, S. P., *Théorie des plaques et coques* (Paris, Dunod, 1968).
[20] Derail, C., Doctoral Thesis, Université de Pau (1995).
[21] Gent, A. N. and Hamed, G. R., *J. Appl. Polym. Sci.* **21**, 2817 (1977).
[22] Bernstein, B., Kearsley, E. A. and Zapas, L. J., *Trans. Soc. Rheol.* **7**, 391 (1963).
[23] Lodge, A. S., *Elastic Liquids* (Academic Press, New York, 1964).
[24] Wagner, M. H., *Rheol. Acta.* **18**, 681 (1979).
[25] Mizumachi, H., *J. Appl. Polym. Sci.* **30**, 2675 (1985).